International Journal of Solids and Structures 46 (2009) 1911–1924

Contents lists available at ScienceDirect

International Journal of Solids and Structures

journal homepage: www.elsevier.com/locate/ijsolstr

# A micromechanical model for predicting thermal properties and thermo-viscoelastic responses of functionally graded materials

Anastasia H. Muliana *

*Department of Mechanical Engineering, Texas A&M University, College Station, TX 77843-3123, USA*

ARTICLE INFO

*Article history:*
Received 19 September 2008
Received in revised form 11 December 2008
Available online 21 January 2009

*Keywords:*
Micromechanics
Thermal properties
Viscoelastic
Functionally graded materials

ABSTRACT

This study introduces a micromechanical model for predicting effective thermo-viscoelastic behaviors of a functionally graded material (FGM). The studied FGM consists of two constituents with varying compositions through the thickness. The microstructure of the FGM is idealized as solid spherical particles spatially distributed in a homogeneous matrix. The mechanical properties of each constituent can vary with temperature and time, while the thermal properties are allowed to change with temperature. The FGM model includes a transition zone where the inclusion and matrix constituents are not well defined. At the transition zone, an interchange between the two constituents as inclusion and matrix takes place such that the maximum inclusion volume contents before and after the transition zone are less than 50%. A micromechanical model is used to determine through-thickness effective thermal conductivity, coefficient of thermal expansion, and time-dependent compliance/stiffness of the FGM. The material properties at the transition zone are assumed to vary linearly between the two properties at the bounds of the transition zone. The micromechanical model is designed to be compatible with finite element (FE) scheme and used to analyze heat conduction and thermo-viscoelastic responses of FGMs. Available experimental data and analytical solutions in the literature are used to verify the thermo-mechanical properties of FGMs. The effects of time and temperature dependent constituent properties on the overall temperature, stress, and displacement fields in the FGM are also examined.

© 2009 Elsevier Ltd. All rights reserved.

## 1. Introduction

Functionally graded materials (FGMs) were first developed in Japan, in the mid-80s, and were used in thermal protection components in the space shuttle. FGMs are engineered materials having non-uniform spatial variations of microstructures and compositions of the constituents that continuously or discretely change the mechanical and physical macroscopic properties. FGMs with various gradations of metal and ceramic constituents are commonly used for extreme temperature applications, in which they can be subjected to a temperature gradient of 1000 K along a thickness of 1 cm. By tailoring thermal protection coatings to form gradual variations in the compositions of the constituents, it is expected that the stress discontinuities at the interphases between the dissimilar constituents can be reduced and delamination between the coatings and the host structures (substrates) can be avoided. Other constituents, such as polymer, carbon, glass, and boron, have also been considered for use in FGMs. Under extreme temperature changes and complex mechanical loadings, the mechanical and physical properties of constituents in the FGMs can vary with the temperature and deformation fields (nonlinear responses) and some of the constituents might exhibit pronounced time-dependent behaviors.

Analytical and numerical solutions for coupled problems of heat transfers and thermo-elastic deformations in FGMs have been obtained. Spatial variations in effective thermal and mechanical properties are often expressed using rule of mixtures based on polynomial functions of the volume contents of the constituents. Noda (1999) derived closed form solutions for thermal stress fields of the FGM plates subject to through-thickness steady heat conduction. Crack propagation and stress intensity factor in FGM due to thermal shock were determined. It was concluded that a proper selection of the constituent variations in the FGM could reduce both thermal stresses and stress intensity factors in cracked FGM. Shen and Noda (2005) presented postbuckling analyses of an FGM cylinder undergoing radial heat conduction combined with axial loads and external surface pressures. The thermal and elastic properties of the constituents were allowed to vary with the temperature fields. Parametric studies showed that the postbuckling responses of the FGM depend strongly on the material gradation in the FGM cylinders. Reddy and co-authors (1998a,b, 1999) have formulated numerical solutions within finite element (FE) schemes for analyzing coupled heat transfers and thermo-elastic deformations in FGM plates and cylinders. The thermal and elastic properties of the constituents were assumed to follow cubic polynomial

* Tel.: +1 979 458 3579; fax: +1 979 845 3081.
*E-mail address:* amuliana@neo.tamu.edu

0020-7683/$ - see front matter © 2009 Elsevier Ltd. All rights reserved.
doi:10.1016/j.ijsolstr.2009.01.008

functions of temperatures. Reddy and Chin (1998) have also investigated the effects of thermo-mechanical coupling on the responses of FGM plates and cylinders. They suggested that the thermo-mechanical coupling has significant effects on the stress fields of FGM under high temperature loadings.

Optimization in microstructural compositions of FGM is necessary to reduce thermal stresses and improve performance of the FGM. Micromechanics based models have been formulated to analyze linear thermo-elastic responses of FGMs. Aboudi et al. (1996, 1999) and Pindera et al. (2002) presented higher order micromechanical models for analyzing steady linear heat conduction and thermo-elastic deformations of FGMs. FGMs with one, two, and three graded directions were studied. A micromechanical model based on the method of cells was used to obtain effective spatial variations in the field quantities. Higher order functions of the field quantities were defined for each constituent. Closed form solutions of stress and deformation fields in the FGM beams and plates obtained from the higher order theory were comparable to the ones calculated using FE. Ostoja-Starzewski et al. (1996) presented micromechanical models to determine effective linear thermal conductivity and linear elastic constants of FGM fiber reinforced composites. The solutions depended on three scales: the fine structures of interphase region, fiber size and spacing, and macroscopic dimension of the composites. The interphase region between fiber and matrix was modeled as a finite region having random arrangements of fiber and matrix. Mori–Tanaka's model and self-consistent micromechanical models have been used to analyze thermo-elastic responses of FGM, e.g., Reiter et al. (1997), Reddy and Cheng (2001) and Vel and Batra (2003). The thermo-elastic properties of the constituents in the above studies were assumed constant. Reiter et al. (1997) concluded that the elastic responses of the graded microstructures, consisting of well defined continuous matrix and discontinuous inclusions, were better approximated by the Mori–Tanaka model. At the transition zone, where the inclusions and matrix are not well defined, the self-consistent micromodel gave better approximations. Gasik (1998) derived a micromechanical model for analyzing FGMs with arbitrary distributions of the constituents. The FGM microstructures were idealized by piecewise homogeneous materials (subcells) having cubic inclusions. Each subcell corresponded to fixed volume content. The calculated effective elastic constant and coefficient of thermal expansion were compared with the ones obtained using Mori–Tanaka, Voigt, and Kerner's models. Ueda and Gasik (2000) and Ueda (2002) have extended the Gasik (1998) micromodel to analyze transient heat conduction and thermal stresses in FGMs having elastic and inelastic constituents. Parametric studies on the effects of material gradations on the overall stress and deformation fields were performed. Yin et al. (2004, 2007) formulated effective linear coefficient of thermal expansion and effective elastic material constants, i.e., Young's moduli and Poisson's ratio, of FGMs using micromechanical models. The particle interactions were considered in obtaining the effective material properties. The properties of the constituents were assumed *independent* on temperature fields (linear behaviors). The calculated effective material properties were verified with experimental data. It was shown that particle interactions needed to be considered when the volume contents of the particles were relatively high. Shabana and Noda (2008) presented plane stress homogenization schemes for analyzing thermo-elastic responses for functionally graded fiber reinforced composites. Two unit-cell models were defined, i.e., square and hexagonal arrangements. The effective properties calculated from the unit-cell models were implemented in finite elements. The proposed model was verified with experimental data on $ZrO_2$/Ti–6Al4V FGMs.

To the best of my knowledge, studies of FGM with time-dependent material properties are limited. Yang (2000) presented closed form solutions of stress fields in FG cylinders under creep. Hypothetical material properties were studied. Instead of solving a heat conduction equation, radial distributions of temperatures were assumed to follow the power law function of the cylinder's radius. The multi-axial stress–strain rates followed Norton's creep model and the strain–displacement and equilibrium relations of the linear elastic cylinder were directly applied to the stress–strain rates. Zhou and Hashida (2001, 2002) and Zhai et al. (2005) studied the effect of creep on the overall responses and properties of FGMs. They showed that the residual stresses in the FGM due to high temperature loadings could cause significant creep responses. Mukherjee and Paulino (2003) used correspondence principle for analyzing linear viscoelastic responses of FGMs. Maxwell spring-dashpot mechanical analog model, which is suitable for viscoelastic fluid model, was used for modeling the spatial relaxation moduli. They also discussed that the correspondence principle fails in modeling the viscoelastic responses of FGM when the time and location dependent functions cannot be separated and expressed in a product form.

This study presents a micromechanical model for predicting effective thermo-viscoelastic behaviors of FGMs graded in one direction. The studied FGM consists of two constituents. The microstructures of the FGM are assumed to be solid spherical particles spatially distributed in a homogeneous matrix. At the transition zone, where the inclusion and matrix constituents are not well defined, there is an interchange between the inclusion and matrix constituents. At the structural level, continuum finite elements with multiple integration points through the element's thickness are used. A micromechanical model is formulated to obtain effective thermal conductivity, coefficient of thermal expansion, and time-dependent compliance/stiffness. These effective properties, which vary through the thickness, are sampled at the integration points within the continuum elements. It is also possible to implement the micromodel within shell, plate, membrane, and other types of elements in the FE analyses. The mechanical properties of each constituent are allowed to vary with temperature and time while the thermal properties depend on the temperature. Available experimental data and analytical solutions in the literature are used to verify the thermo-mechanical properties of the FGMs derived in this study. The manuscript is organized as follows. Section 2 presents constitutive equations for the thermo-viscoelastic responses of isotropic constituents in the FGM. Section 3 describes a micromechanical model for obtaining effective nonlinear thermal and viscoelastic properties of the FGM. Section 4 discusses numerical implementation and verification of the micromechanical model. The effects of time and temperature dependent constituent properties on the overall temperature, stress, and displacement fields in the FGM are also examined.

## 2. Constitutive equations for thermo-viscoelastic responses of isotropic constituents

The following constitutive relation for linearized thermo-viscoelastic deformations of solids (non-aging materials) is used for the constituents:

$$\varepsilon_{ij}(t) = \int_0^t S_{ijkl}(T^\tau, \psi^t - \psi^\tau)\frac{\partial \sigma_{kl}(\tau)}{\partial \tau}d\tau + \int_0^t \alpha_{ij}(T^\tau)\frac{\partial \Delta T(\tau)}{\partial \tau}d\tau \qquad (1)$$

where $\boldsymbol{S}$ is the creep compliance tensor that depends on temperature; and $\boldsymbol{\alpha}$ is the temperature-dependent coefficient of linear thermal expansion (CTE) tensor. At reference temperature, To the constituent is assumed to be stress-free and its properties are independent of the temperatures (constant). The linearized strain is defined by $\varepsilon_{ij} = \frac{1}{2}[u_{i,j} + u_{j,i}]$, where $\boldsymbol{u}$ is the displacement. The time and temperature dependent compliance is expressed by:

$$S_{ijkl}(t,T) = S_{ijkl}(0,T) + \Delta S_{ijkl}(t,T) \tag{2}$$

where $\boldsymbol{S}(0,T)$ is the compliance at time 0, which is often considered as the time independent (instantaneous elastic) compliance, and $\Delta\boldsymbol{S}(t,T)$ is the transient time-dependent compliance. The temperature $T$ in the compliance tensor can vary with time. Substituting Eq. (2) into Eq. (1) gives:

$$\varepsilon_{ij}(t) = \varepsilon^M_{ij}(t) + \varepsilon^T_{ij}(t)$$

$$\begin{aligned}\varepsilon_{ij}(t) &= \int_0^t [S_{ijkl}(0,T^\tau) + \Delta S_{ijkl}(t-\tau,T^\tau)]\frac{d\sigma_{kl}(\tau)}{d\tau}d\tau \\ &\quad + \int_0^t \alpha_{ij}(T^\tau)\frac{d\Delta T(\tau)}{d\tau}d\tau \\ &= S_{ijkl}(0,T^t)\sigma_{kl}(t) + \int_0^t \Delta S_{ijkl}(t-\tau,T^\tau)\frac{d\sigma_{kl}(\tau)}{d\tau}d\tau \\ &\quad + \int_0^t \alpha_{ij}(T^\tau)\frac{d\Delta T(\tau)}{d\tau}d\tau\end{aligned} \tag{3}$$

The temperature-dependent creep function is expressed as:

$$S_{ijkl}(t,T) = g(T^t)S_{ijkl}(0) + f(T^t)\Delta S_{ijkl}(\psi^t) \tag{4}$$

The transient compliance in Eq. (4) follows the Prony series exponential form, which is:

$$\Delta S^{\psi^t}_{ijkl} = \sum_{n=1}^{N_{ijkl}} S_{ijkl(n)}\left(1 - \exp[-\lambda_{ijkl(n)}\psi^t]\right) \tag{5}$$

where $N_{ijkl}$ is the number of terms for each component in the transient compliance tensor, $S_{ijkl(n)}$ is the $n$th coefficient of the Prony series for each component in the transient compliance, and $\lambda_{ijkl(n)}$ is the $n$th reciprocal of retardation time that corresponds to $S_{ijkl(n)}$. The expression of the reduced time function $\psi^t$ in Eq. (5) can be found in many articles on viscoelasticity, e.g., Wineman and Rajagopal (2001), and is given as:

$$\psi^t \equiv \psi(t) = \int_0^t \frac{d\xi}{a(T^\xi)} \tag{6}$$

The constitutive relation in Eq. (3) can be easily reduced to isotropic viscoelastic materials, which has been studied previously (Haj-Ali and Muliana, 2004; Muliana and Khan, 2008; Sawant and Muliana, 2008). It is also assumed that the corresponding linear elastic Poisson's ratio for the viscoelastic solid is constant. Thus, the extensional, $D(t)$, shear, $J(t)$, and bulk, $B(t)$ linear creep compliances share the same creep function, which are expressed as:

$$\begin{aligned}&D(t) = D(0) + \Delta D(\psi^t) \\ &J(t) = J(0) + \Delta J(\psi^t) \quad J(0) = 2(1+\nu)D(0) \\ &B(t) = B(0) + \Delta B(\psi^t) \quad B(0) = 3(1-2\nu)D(0) \\ &\Delta D^{\psi^t} \equiv \Delta D(\psi^t) = \sum_{n=1}^{N} D_n(1 - \exp[-\lambda_n\psi^t]) \\ &\Delta J^{\psi^t} \equiv \Delta J(\psi^t) = \sum_{n=1}^{N} J_n(1 - \exp[-\lambda_n\psi^t]) \quad J_n = 2(1+\nu)D_n \\ &\Delta B^{\psi^t} \equiv \Delta B(\psi^t) = \sum_{n=1}^{N} B_n(1 - \exp[-\lambda_n\psi^t]) \quad B_n = 3(1-2\nu)D_n\end{aligned} \tag{7}$$

The integral model for the mechanical strain component in Eq. (1) can now be applied separately for the deviatoric and volumetric strains. The total strain is written as:

$$\begin{aligned}\varepsilon^t_{ij} &= \varepsilon_{ij}(t) \\ &= \int_0^t J(T^\tau,(\psi^t - \psi^\tau))\frac{\partial S^\tau_{ij}}{\partial\tau}d\tau + \delta_{ij}\int_0^t B(T^\tau,(\psi^t-\psi^\tau))\frac{\partial\sigma^\tau_{kk}}{\partial\tau}d\tau \\ &\quad + \delta_{ij}\int_0^t \alpha(T^\tau)\frac{\partial\Delta T^{(\tau)}}{\partial\tau}d\tau\end{aligned} \tag{8}$$

where $S_{ij}$ and $\sigma_{kk}$ are the components of the deviatoric and volumetric stress tensors, respectively. Superscript $t$ indicates the variable at time $t$. A recursive method is used to solve the convolution integral forms with temperature-dependent material properties. Detailed formulation of the recursive integration scheme can be found in Muliana and Khan (2008). A consistent tangent stiffness matrix is determined by taking the inverse of the partial derivative of the incremental strain with respect to the incremental stress at the end of each time step. The consistent tangent stiffness, $C^t_{ijkl}$, at the converged state, is:

$$C^t_{ijkl} \equiv \frac{\partial\Delta\sigma^t_{ij}}{\partial\Delta\varepsilon^{M,t}_{kl}} = \left[\frac{\partial\Delta\varepsilon^{M,t}_{ij}}{\partial\Delta\sigma^t_{kl}}\right]^{-1} \quad \text{where} \quad \bar{\boldsymbol{S}} = \left[\frac{\partial\Delta\boldsymbol{\varepsilon}^{M,t}}{\partial\Delta\boldsymbol{\sigma}^1}\right]^{-1} \tag{9}$$

An incremental scalar component of the thermal strain is:

$$T^t \equiv T^{t-\Delta t} + \Delta T^t \qquad \Delta\varepsilon^{T,t}_{ij} \equiv \alpha(T^t)\Delta T^t\delta_{ij} \tag{10}$$

where $\alpha(T^t)$ is the temperature dependent coefficient of thermal expansion scalar and $\delta_{ij}$ is the Kronecker delta.

The Fourier's heat flux equation is used for the isotropic constituents and is defined by:

$$q^t_i \equiv q_i(T,x_k,t) = -\int_0^t k(T^\tau)\frac{\partial\varphi_i}{\partial\tau}d\tau \quad i,k = 1,2,3 \tag{11}$$

where $k^t \equiv k(T^t)$ is the temperature-dependent thermal conductivity, $x_k$ is the position of the material point, $t$ is the current time, and $\varphi_i \equiv T_{,i}$ is the component of the temperature gradient. A general energy equation for a linearized thermo-mechanical deformation without internal heating and heat generation from the dissipation of energy is given as (Boley and Weiner, 1997):

$$\rho c\dot{T} = -q^t_{i,i} \tag{12}$$

where $\rho$ is the material density and $c$ is the specific heat at a constant deformation. In general, both $\rho$ and $c$ can be temperature dependent. In order to implement the heat conduction in a displacement based FE at the macro-level, Eqs. (11) and (12) are solved incrementally. A backward finite difference algorithm is used within an incremental time-step. The left-hand side of the energy equation in Eq. (12) is approximated by:

$$\rho c\dot{T} \approx \frac{\rho c}{\Delta t}(T^t - T^{t-\Delta t}) = \frac{\rho c}{\Delta t}\Delta T^t \tag{13}$$

The temperature and temperature gradient at the current time are expressed as:

$$\begin{aligned}&T^t = T^{t-\Delta t} + \Delta T^t \\ &\varphi^t_i = \varphi^{t-\Delta t}_i + \Delta\varphi^t_i \quad \text{where } \Delta\varphi^t_i = \Delta T^t_{,i}\end{aligned} \tag{14}$$

The heat flux at current time $t$ is then defined as:

$$\begin{aligned}&q^t_i = q^{t-\Delta t}_i + \Delta q^t_i \\ &\Delta q^t_i = -k^t\Delta\varphi^t_i\end{aligned} \tag{15}$$

Since the thermal conductivity depends on temperature, the constitutive equation is solved iteratively to obtain correct solutions to the thermal constitutive behavior. It is then necessary to define variations of the heat flux with respect to temperature at the end of increment, which is:

$$\frac{\partial q_i^t}{\partial T^t} = -\frac{\partial k^t}{\partial T^t}\varphi_i^t \tag{16}$$

## 3. Micromechanical model formulations for FGMs

This section presents the integrated micromechanical and FE structural framework, illustrated in Fig. 1, for analyzing thermo-viscoelastic behaviors of FGMs. The studied FGMs are made of two constituents. A three-dimensional continuum element with multiple integration (material) points through the thickness is used at the structural level. Spatial variations in the macroscopic material properties that are determined by the compositions and microstructures of the constituents are implemented at the integration points. A simplified microstructure of the FGM panel, having particles distributed in a homogeneous matrix, is also shown in Fig. 1. It is assumed that the through-thickness material variation can be represented with piecewise homogeneous media. The effective thermo-viscoelastic properties for each homogenous composite medium are obtained using a micromodel of particle reinforced composites. The through-thickness variations of the volume fractions of the two constituents are given as:

$$v_f^1 = \left(1 - \frac{z}{h}\right)^n \qquad v_f^2 = 1 - \left(\frac{h-z}{h}\right)^n \tag{17}$$

where $z$ is the through-thickness locations and $n$ defines the graded variations. Along with the gradation in the composition of the two constituents, there is an interchange between the inclusion and matrix constituents, illustrated in Fig. 2. The interchange takes place at the transition zone, where interpenetrating between the constituents can be observed. Below the transition zone, constituent 2 acts as a discontinuous inclusion and constituent 1 acts as a continuous matrix. Above the transition zone, constituent 1 is an inclusion dispersed in matrix medium of constituent 2.

The overall responses of composites depend on their microstructural details, i.e., stiff inclusions in a soft matrix or soft inclusions in a stiff matrix. Furthermore, as volume contents of inclusions increase, there often exists particle interaction/contact. This interaction can significantly affect the overall responses of composites. The rule of mixture approach is not capable of incorporating these effects as the effective properties obtained using the rule of mixture are mainly proportional to the volume contents of the constituents. In this study, the roles of the constituents as inclusion and matrix are explicitly accounted for to determine the effective nonlinear thermo-viscoelastic properties of the FGM. The effects of the inclusion and matrix constituents on the effective thermo-viscoelastic properties of composites will be discussed in Section 4. The volume fractions of the two inclusions in the FGM graded in $z$-direction (Fig. 2) are given by:

$$\begin{aligned} v_{\mathrm{pf}}^2 &= 1 - \left(1 - \tfrac{z}{h}\right)^n \quad z \leqslant h_1 \qquad v_{\mathrm{pf}}^1 = \left(\tfrac{h-z}{h}\right)^n \quad z \geqslant h_2 \\ 0.0 &\leqslant v_{\mathrm{pf}}^2 < 0.5 \qquad\qquad 0.0 \leqslant v_{\mathrm{pf}}^1 < 0.5 \end{aligned} \tag{18}$$

It is also possible to pick different nonlinear functions to represent the variations in the constituent compositions along the graded directions. The transition zone should be properly characterized from experimental tests, which will be discussed in Section 4. Since the inclusion and matrix constituents in the transition zone are not well defined and there may be interpenetrating between the two constituents, effective thermo-viscoelastic properties at this zone cannot be determined using the present micromechanical model. However, to provide continuous variations in material properties, instead of obtaining rigorous physical based model for the transition zone, this study assumes that the properties at the transition

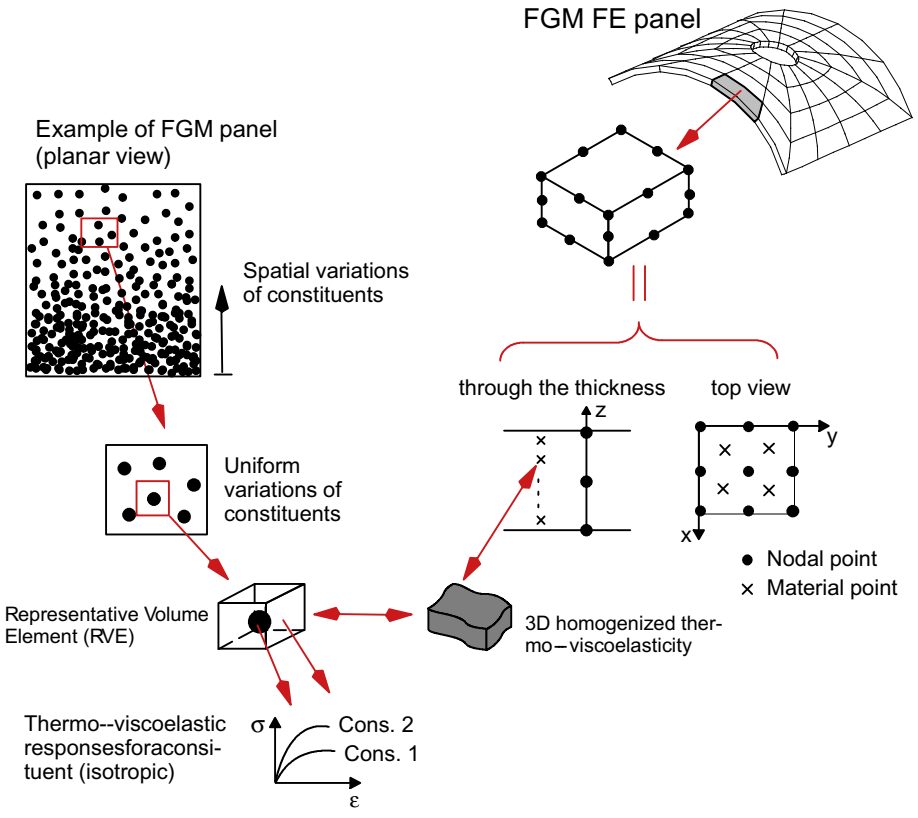


**Fig. 1.** Integrated micromechanical–structural framework of functionally graded materials (FGM).

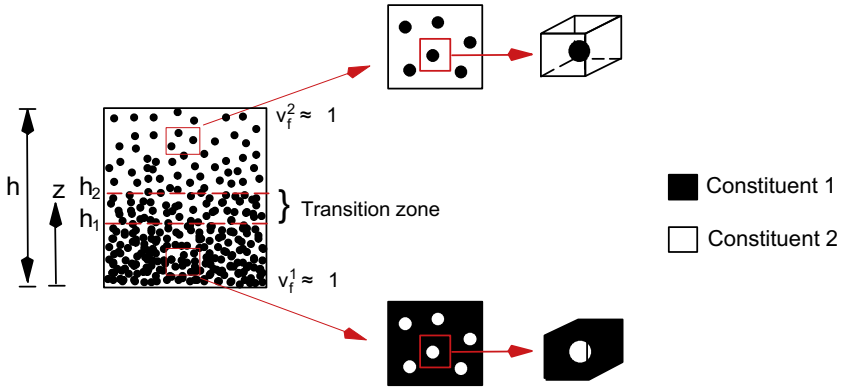


**Fig. 2.** Three regions of FGM graded in one direction.

zone vary linearly between the two properties at $h_1$ and $h_2$, expressed as:

$$\overline{\mathbf{P}}(z) = \overline{\mathbf{P}}(h_1) + \frac{\overline{\mathbf{P}}(h_2) - \overline{\mathbf{P}}(h_1)}{h_2 - h_1} z \qquad h_1 < z < h_2 \tag{19}$$

where $\overline{\mathbf{P}}$ is the effective material properties at the transition zone. It is also possible to define nonlinear functions for the variations in the effective thermo-mechanical properties at the transition zone, as previously studied by Reiter et al. (1997) and Yin et al. (2004, 2007). In order to obtain more detailed effective properties at the transition zone, rigorous physical-based models that incorporate phase interactions, e.g., Alberola and Mele (1996) and Torquato (2002), can be used.

### 3.1. Micromechanical models for effective CTE and moduli of viscoelastic composites

Exact solutions of deformations and transport mechanisms in heterogeneous materials can be theoretically obtained by solving boundary value problems. Depending on the complexity of the problems, finding exact closed form solutions can be cumbersome. This study uses a simplified micromechanical model of particle reinforced composites to determine local CTE and moduli of FGM having temperature and time dependent properties of the constituents. A micromechanical model developed by Muliana and Kim (2007) for stress-dependent viscoelastic composites is modified to incorporate the thermal effects. Several fundamental assumptions are made. A microstructure is defined by a representative volume element (RVE) that is uniformly repeatable over entire composite media and the RVE's length scale is much smaller than the macrostructural scale. The geometry representation of the RVE is similar to the one studied by Aboudi and co-authors (1996, 1999, 2002) for FGM with nonuniform particle spacing. A periodic boundary condition is imposed to the RVE. Field quantities on the boundary of the RVE are defined as field quantities of the homogenized composite media. It is also assumed that the RVE is much larger compared to the atomistic scale, such that the use of continuum mechanics approach remains valid.

A unit-cell model consisting of four particle and matrix subcells (Muliana and Kim, 2007) is used to obtain effective properties. The unit-cell model is illustrated in Fig. 3. Average stresses and strains represent the effective quantities of fictitious homogeneous media. The average stresses and strains in the unit-cell model are defined by:

$$\bar{\sigma}_{ij} = \frac{1}{V}\sum_{\beta=1}^{N}\int_{V^{(\beta)}} \sigma_{ij}^{(\beta)}\left(x_k^{(\beta)}\right) dV^{(\beta)} \approx \frac{1}{V}\sum_{\beta=1}^{N} V^{(\beta)}\sigma_{ij}^{(\beta)} \tag{20}$$

$$\bar{\varepsilon}_{ij} = \frac{1}{V}\sum_{\beta=1}^{N}\int_{V^{(\beta)}} \varepsilon_{ij}^{(\beta)}\left(x_k^{(\beta)}\right) dV^{(\beta)} \approx \frac{1}{V}\sum_{\beta=1}^{N} V^{(\beta)}\varepsilon_{ij}^{(\beta)} \tag{21}$$

Superscript $(\beta)$ denotes the subcell number and $N$ is the number of subcells. The stress $\sigma_{ij}^{(\beta)}$ and strain $\varepsilon_{ij}^{(\beta)}$ are the average stress and strain within each subcell. The unit-cell volume $V$ is $V = \sum_{\beta=1}^{N} V^{(\beta)}$.

Eqs. (20) and (21) are exact only for linear thermo-elastic responses of composites. Due to the nonlinear and time-dependent

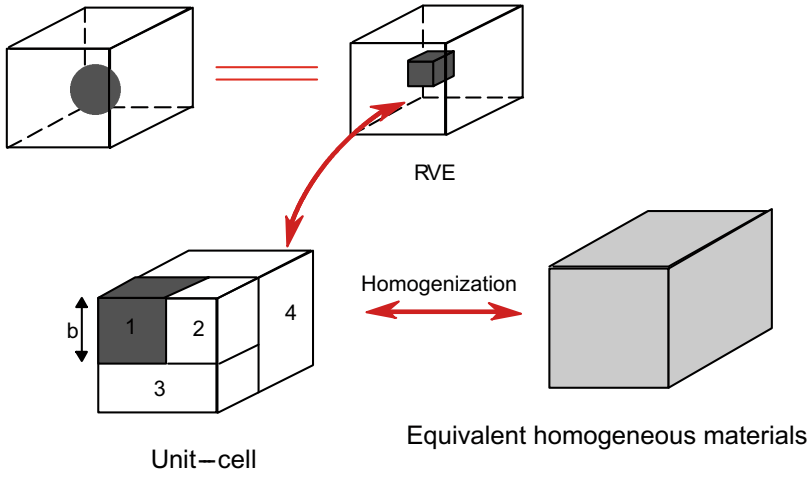


**Fig. 3.** Representative unit-cell model for particulate reinforced polymers.

responses in the constituents, the solutions for the deformation fields are performed incrementally. The incremental forms of the effective stress and strain tensors at the current time are:

$$\begin{aligned}\bar{\sigma}_{ij}^{t} &= \bar{\sigma}_{ij}^{t-\Delta t} + \Delta\bar{\sigma}_{ij}^{t} \\ \bar{\varepsilon}_{ij}^{t} &= \bar{\varepsilon}_{ij}^{t-\Delta t} + \Delta\bar{\varepsilon}_{ij}^{t}\end{aligned} \tag{22}$$

The average stress and strain tensors in the subcells are given as:

$$\begin{aligned}\sigma_{ij}^{(\beta),t} &= \sigma_{ij}^{(\beta),t-\Delta t} + \Delta\sigma_{ij}^{(\beta),t} \\ \varepsilon_{ij}^{(\beta),t} &= \varepsilon_{ij}^{(\beta),t-\Delta t} + \Delta\varepsilon_{ij}^{(\beta),t}\end{aligned} \tag{23}$$

Superscript $(t-\Delta t)$ denotes previous converged solutions and prefix $\Delta$ indicates incremental variables within a current time increment $\Delta t$. A linearized relation is first imposed to the incremental parts of the stress and strain tensors in Eqs. (22) and (23). An iterative corrector scheme is then performed to satisfy both the micromechanical constraints and the nonlinear thermo-viscoelastic constitutive equations.

Fourth order strain-concentration tensors ($\boldsymbol{B}^{(\beta),t}$), which relate the subcell average strains, $\Delta\boldsymbol{\varepsilon}^{(\beta),t}$, to the composite effective strain, $\Delta\bar{\boldsymbol{\varepsilon}}^{t}$, are also defined. This is written as:

$$\Delta\varepsilon_{ij}^{(\beta),t} = B_{ijkl}^{(\beta),t}\Delta\bar{\varepsilon}_{kl}^{t} \tag{24}$$

Since the RVE's length scale is much smaller than the FGM's macroscale, it is assumed that the temperature changes within a time increment $\Delta t$ at each subcell ($\Delta T^{(\beta),t}$) in a unit-cell model is equal to the effective temperature change at the boundary of the RVE ($\Delta\overline{T}^{t}$). This is written as:

$$\Delta T^{(\beta),t} = \Delta\overline{T}^{t} \tag{25}$$

Using the incremental strain and the incremental temperature defined in Eqs. (24) and (25), a constitutive equation for each subcell can be expressed as:

$$\begin{aligned}\Delta\sigma_{ij}^{(\beta),t} &= C_{ijkl}^{(\beta),t}\left[\Delta\varepsilon_{kl}^{(\beta),t} - \alpha_{kl}^{(\beta),t}\Delta T^{(\beta)t}\right] \\ &= C_{ijkl}^{(\beta),t}\left[B_{klrs}^{(\beta),t}\Delta\bar{\varepsilon}_{rs}^{t} - \alpha_{kl}^{(\beta),t}\Delta\overline{T}^{t}\right]\end{aligned} \tag{26}$$

where $\boldsymbol{C}^{(\beta),t}$ is the consistent tangent stiffness matrix of each subcell at a current time $t$ which is defined in Eq. (9). Substituting Eq. (26) into an incremental form of Eq. (20) gives:

$$\Delta\bar{\sigma}_{ij}^{t} = \frac{1}{V}\sum_{\beta=1}^{N} V^{(\beta)}C_{ijkl}^{(\beta),t}\left[B_{klrs}^{(\beta),t}\Delta\bar{\varepsilon}_{rs}^{t} - \alpha_{kl}^{(\beta),t}\Delta\overline{T}^{t}\right] \tag{27}$$

The effective tangent stiffness matrix $\overline{\boldsymbol{C}}^{t}$ for the composites is determined by:

$$\overline{C}_{ijrs}^{t} = \frac{1}{V}\sum_{\beta=1}^{N} V^{(\beta)}C_{ijkl}^{(\beta),t}B_{klrs}^{(\beta),t} \tag{28}$$

In order to derive strain-concentration matrices for all subcells, the micromechanical relations together with the subcells constitutive material models must be imposed. Detailed micromechanical relations and formulations of the $\boldsymbol{B}^{(\beta),t}$ matrices are given in Muliana and Kim (2007) and Muliana and Sawant (in press). The homogenized properties in the micromodel are derived by assuming perfect bond along the interfaces of the subcells and imposing displacement compatibility and traction continuity at the subcells' interface. The effective stress–strain relations for the particle reinforced composites (Fig. 3) are then rewritten as:

$$\begin{aligned}\Delta\bar{\sigma}_{ij}^{t} &= \overline{C}_{ijkl}^{t}\Delta\bar{\varepsilon}_{kl}^{t} \\ &\quad - \frac{\Delta\overline{T}^{t}}{V}\left[V^{(A)}C_{ijkl}^{(A),t}\alpha_{kl}^{(A),t} + V^{(3)}C_{ijkl}^{(3),t}\alpha_{kl}^{(3),t} + V^{(4)}C_{ijkl}^{(4),t}\alpha_{kl}^{(4),t}\right] \\ &= \overline{C}_{ijkl}^{t}\left[\Delta\bar{\varepsilon}_{kl}^{t} - \Delta\overline{T}^{t}\bar{\alpha}_{kl}^{t}\right]\end{aligned} \tag{29}$$

where $V^{(A)} = V^{(1)} + V^{(2)}$. The effective tangent CTE in Eq. (29), for the isotropic case, is then expressed as:

$$\begin{aligned}\bar{\alpha}_{ij}^{t} &= \bar{\alpha}^{t}\delta_{ij} \\ &= \frac{\overline{C}_{ijkl}^{t,-1}}{V}\left[V^{(A)}C_{klmn}^{(A),t}\alpha_{mn}^{(A),t} + V^{(3)}C_{klmn}^{(3),t}\alpha_{mn}^{(3),t} + V^{(4)}C_{klmn}^{(4),t}\alpha_{mn}^{(4),t}\right]\end{aligned} \tag{30}$$

where $\alpha_{ij}^{(A),t}$ and $\overline{C}_{ijkl}^{(A),t}$ in Eq. (30) are defined by:

$$\alpha_{ij}^{(A),t} = \alpha^{(A),t}\delta_{ij} = \frac{1}{V^{(A)}}\left[V^{(1)}\alpha_{ij}^{(1),t} + V^{(2)}\alpha_{ij}^{(2),t}\right] \tag{31}$$

$$C_{ijkl}^{(A),t} = X_{ijkl}^{t,-1} \quad \text{and} \quad X_{ijkl}^{t} = \frac{1}{V^{(A)}}\left(V^{(1)}C_{ijkl}^{(1),t-1} + V^{(2)}C_{ijkl}^{(2),t-1}\right) \tag{32}$$

It is seen that the effective CTE in Eq. (30) depends on the elastic material constant and CTE of each constituent. Thus, for the temperature dependent constituent mechanical and thermal properties, the effective CTE can change with temperatures. In case of viscoelastic constituents are considered, the effective CTE also changes with time.

### 3.2. Micromechanical models for effective thermal conductivity in composites

The effective heat flux, defined based on a volume averaging method, is written as:

$$\bar{q}_i = \frac{1}{V}\sum_{\beta=1}^{N}\int_{V^{(\beta)}} q_i^{(\beta)}\left(x_k^{(\beta)}\right)dV^{(\beta)} \approx \frac{1}{V}\sum_{\beta=1}^{N} V^{(\beta)}q_i^{(\beta)} \quad i,k = 1,2,3 \tag{33}$$

where $q_i^{(\beta)}$ is the component of the heat flux in the subcell $(\beta)$. The Fourier's heat flux equation is used and is written as:

$$\bar{q}_i = -\bar{k}_{ij}\bar{\varphi}_j \quad \text{where} \quad \bar{\varphi}_j = \frac{\partial\overline{T}}{\partial x_j} \tag{34}$$

where $\bar{\boldsymbol{k}}$ and $\bar{\boldsymbol{\varphi}}$ are the effective thermal conductivity and temperature gradient, respectively. When the thermal conductivity of each constituent is allowed to change with the temperature field and the temperature field at current time is yet to be solved, an iterative method within an incremental formulation is used to determine the effective heat flux. This is written as:

$$\begin{aligned}\bar{q}_i^{t} &= \bar{q}_i^{t-\Delta t} + \Delta\bar{q}_i^{t} \\ \overline{T}^{t} &= \overline{T}^{t-\Delta t} + \Delta\overline{T}^{t}\end{aligned} \tag{35}$$

The homogenized relation in Eq. (33) is applied to the incremental parts of the heat flux and temperature gradient. Linearized solutions are first obtained within the current incremental time followed by iteration to minimize residual from linearization. In order to determine the temperature field at any time throughout the composite media, $\overline{T}(x_i,t)$, the following linearized heat conduction (energy equation) is solved:

$$\overline{\rho c}\dot{\overline{T}} = -\bar{q}_{i,i} \quad \text{for} \quad i = 1,2,3 \tag{36}$$

It is assumed that the thermo-mechanical coupling, heat generation due to dissipation of energy, and internal heat source are negligible. The conduction of heat and the deformation of materials are coupled as the material properties depend on temperature. The effective heat capacity in Eq. (36) is obtained using a volume averaging method which is expressed as:

$$\overline{\rho c} = \frac{1}{V}\sum_{\beta=1}^{N}\int_{V^{(\beta)}}(\rho c)^{(\beta)}\left(x_k^{(\beta)}\right)dV^{(\beta)} \approx \frac{1}{V}\sum_{\beta=1}^{N} V^{(\beta)}(\rho c)^{(\beta)} \tag{37}$$

The temperature distribution $\overline{T}^{t} \equiv \overline{T}(x_i,t)$ determined by solving Eq. (36) is used as prescribed temperature boundary conditions for the RVE. Due to the assumption that the RVE's length scale is much

smaller than the macrostructural scale, the transient heat conduction is solved only at the composite (macro) level, while a steady state heat conduction is assumed at the microstructural level.

Second order concentration tensors ($\boldsymbol{F}^{(\beta),t}$), which relate the subcell average incremental temperature gradients, $\Delta\boldsymbol{\varphi}^{(\beta),t}$, to the composite incremental effective temperature gradient, $\Delta\bar{\boldsymbol{\varphi}}^{t}$, are defined by:

$$\Delta\varphi_i^{(\beta),t} = F_{ij}^{(\beta),t}\Delta\bar{\varphi}_j^t \tag{38}$$

Using the relation in Eq. (38), an incremental heat flux equation in each subcell is given as:

$$\Delta q_i^{(\beta),t} = -k_{ij}^{(\beta),t}F_{jk}^{(\beta),t}\Delta\bar{\varphi}_k^t \tag{39}$$

Substituting Eq. (33) into (39), the component of the incremental effective heat flux is written as:

$$\Delta\bar{q}_i^t = -\frac{1}{V}\sum_{\beta=1}^{4} V^{(\beta)}k_{ij}^{(\beta),t}F_{jk}^{(\beta),t}\Delta\bar{\varphi}_k^t \tag{40}$$

Thus, the temperature-dependent heat conduction at the current time is expressed as:

$$\bar{k}_{ij}^t = \frac{1}{V}\sum_{\beta=1}^{4} V^{(\beta)}k_{ik}^{(\beta),t}F_{kj}^{(\beta),t} \tag{41}$$

In order to define the concentration tensors ($\boldsymbol{F}^{(\beta),t}$), micromechanical relations and constitutive equations for each constituents are used. The micromechanical relations for the heat flux $\bar{\boldsymbol{q}}^t$ and temperature gradient $\bar{\boldsymbol{\varphi}}^t$ were previously developed by Muliana (2007) which in the incremental forms are expressed as:

$$\begin{aligned}\Delta\bar{q}_i^t &= \left(V^{(1)}+V^{(2)}\right)\Delta q_i^{(A),t} + V^{(3)}\Delta q_i^{(3),t} + V^{(4)}\Delta q_i^{(4),t}\\ \Delta q_i^{(A),t} &= \Delta q_i^{(1),t} = \Delta q_i^{(2),t}\end{aligned} \tag{42}$$

$$\Delta\bar{\varphi}_i^t = \frac{1}{V^{(1)}+V^{(2)}}\left[V^{(1)}\Delta\varphi_i^{(1),t} + V^{(2)}\Delta\varphi_i^{(2),t}\right] = \Delta\varphi_i^{(3),t} = \Delta\varphi_i^{(4),t} \tag{43}$$

The $\mathbf{F}^{(\beta),t}$ matrices are:

$$\mathbf{F}^{(1),t} = \begin{bmatrix} \frac{k_{11}^{(2)}\left(V^{(1)}+V^{(2)}\right)}{V^{(1)}k_{11}^{(2)}+V^{(2)}k_{11}^{(1)}} & 0.0 & 0.0\\ 0.0 & \frac{k_{22}^{(2)}\left(V^{(1)}+V^{(2)}\right)}{V^{(1)}k_{22}^{(2)}+V^{(2)}k_{22}^{(1)}} & 0.0\\ 0.0 & 0.0 & \frac{k_{33}^{(3)}\left(V^{(1)}+V^{(3)}\right)}{V^{(1)}k_{33}^{(3)}+V^{(3)}k_{33}^{(1)}}\end{bmatrix}$$

$$\mathbf{F}^{(2),t} = \begin{bmatrix} \frac{k_{11}^{(1)}\left(V^{(1)}+V^{(2)}\right)}{V^{(1)}k_{11}^{(2)}+V^{(2)}k_{11}^{(1)}} & 0.0 & 0.0\\ 0.0 & \frac{k_{22}^{(1)}\left(V^{(1)}+V^{(2)}\right)}{V^{(1)}k_{22}^{(2)}+V^{(2)}k_{22}^{(1)}} & 0.0\\ 0.0 & 0.0 & \frac{k_{33}^{(4)}\left(V^{(2)}+V^{(4)}\right)}{V^{(2)}k_{33}^{(3)}+V^{(4)}k_{33}^{(2)}}\end{bmatrix}$$

$$\mathbf{F}^{(3),t} = \begin{bmatrix} \frac{k_{11}^{(4)}\left(V^{(3)}+V^{(4)}\right)}{V^{(3)}k_{11}^{(4)}+V^{(4)}k_{11}^{(3)}} & 0.0 & 0.0\\ 0.0 & \frac{k_{22}^{(4)}\left(V^{(3)}+V^{(4)}\right)}{V^{(3)}k_{22}^{(4)}+V^{(4)}k_{22}^{(3)}} & 0.0\\ 0.0 & 0.0 & \frac{k_{33}^{(1)}\left(V^{(1)}+V^{(3)}\right)}{V^{(1)}k_{33}^{(3)}+V^{(3)}k_{33}^{(1)}}\end{bmatrix}$$

$$\mathbf{F}^{(4),t} = \begin{bmatrix} \frac{k_{11}^{(3)}\left(V^{(3)}+V^{(4)}\right)}{V^{(3)}k_{11}^{(4)}+V^{(4)}k_{11}^{(3)}} & 0.0 & 0.0\\ 0.0 & \frac{k_{22}^{(3)}\left(V^{(3)}+V^{(4)}\right)}{V^{(3)}k_{22}^{(4)}+V^{(4)}k_{22}^{(3)}} & 0.0\\ 0.0 & 0.0 & \frac{k_{33}^{(2)}\left(V^{(2)}+V^{(4)}\right)}{V^{(2)}k_{33}^{(4)}+V^{(4)}k_{33}^{(2)}}\end{bmatrix} \tag{44}$$

## 4. Numerical implementation and verification

The present micromechanical model is used to obtain effective thermo-viscoelastic properties and to analyze thermo-viscoelastic behaviors of FGMs. The studied FGM consists of two constituents, acting as a discontinuous inclusion and homogeneous matrix. The compositions of the two constituents vary continuously through the FGM thickness. The FGM model also includes a transition zone where the inclusion and matrix constituents are not well defined. At the transition zone, an interchange between the two constituents as inclusion and matrix occurs. The effects of the microstructural characteristics, i.e., softer inclusion in stiffer matrix or stiffer inclusion in softer matrix, on the through-thickness thermo-elastic properties of the FGM are first examined. The thermal and elastic properties, obtained using the present micromechanical model, are also compared with existing experimental data and the micromechanical model with particle interaction. Finally, the effects of time and temperature dependent constituent properties on the overall heat conduction and deformation of FGM are studied.

### 4.1. Effects of the inclusion and matrix properties

Several micromechanical models have been used to determine local effective properties of the FGM. The variations in the local effective properties are often defined in terms of volume contents of two constituents, which vary from 0 to 1. As the volume content of the inclusion increases, the matrix constituent becomes more discontinuous due to contact between the inclusions. Reiter et al. (1997) have shown that the overall responses of FGMs change with altering the inclusion and matrix constituents, although compositions of the two constituents are kept constant.

This study compares the effective linear elastic properties of the FGM having carbon (C) and silicon carbide (SiC) constituents obtained using the present micromechanical model and the Mori–Tanaka (MT). The properties of the C and SiC constituents are given in Table 1. Fig. 4 illustrates elastic constants of isotropic FGM at various compositions of the SiC constituent. The FGM is assumed to have a linear through-thickness variation of the constituents in which the parameter ($n$) in Eq. (17) is equal to one. The linear elastic properties obtained from the present micromodel are comparable to the ones of the Mori–Tanaka. Slight mismatches are shown for the effective Poisson's ratios and bulk moduli. It is noted that the Poisson's ratios of the two constituents are equal (0.3). The present micromodel gives constant values of the effective Poisson's ratio (0.3), while the MT model shows variations in the effective Poisson's ratio. It is also shown that the FGM through-thickness properties with SiC inclusion and carbon matrix differ than the ones having carbon inclusion and SiC matrix, although the compositions of the two constituents are kept constant. The differences are due to the significant mismatches in the magnitude of the properties of the two constituents. The differences should be expected as the responses of composites having stiff inclusions in a soft matrix differ than the responses of composites with soft inclusions in a stiff matrix. Thus, it is important to properly identify detailed microstructural arrangements, i.e., inclusion and matrix constituents, in predicting effective properties of the FGM. Comparisons of the thermal properties, i.e., effective coefficient of ther-

**Table 1**
Elastic and thermal properties of silicon carbide and carbon (Reiter et al., 1997).

| Constituents | $E$ (GPa) | $\nu$ | $\alpha$ ($10^{-6}$/K) | $k$ (W/mK) |
|---|---|---|---|---|
| Silicon carbide | 320 | 0.30 | 4.2 | 120 |
| Carbon | 28 | 0.30 | 9.3 | 450 |

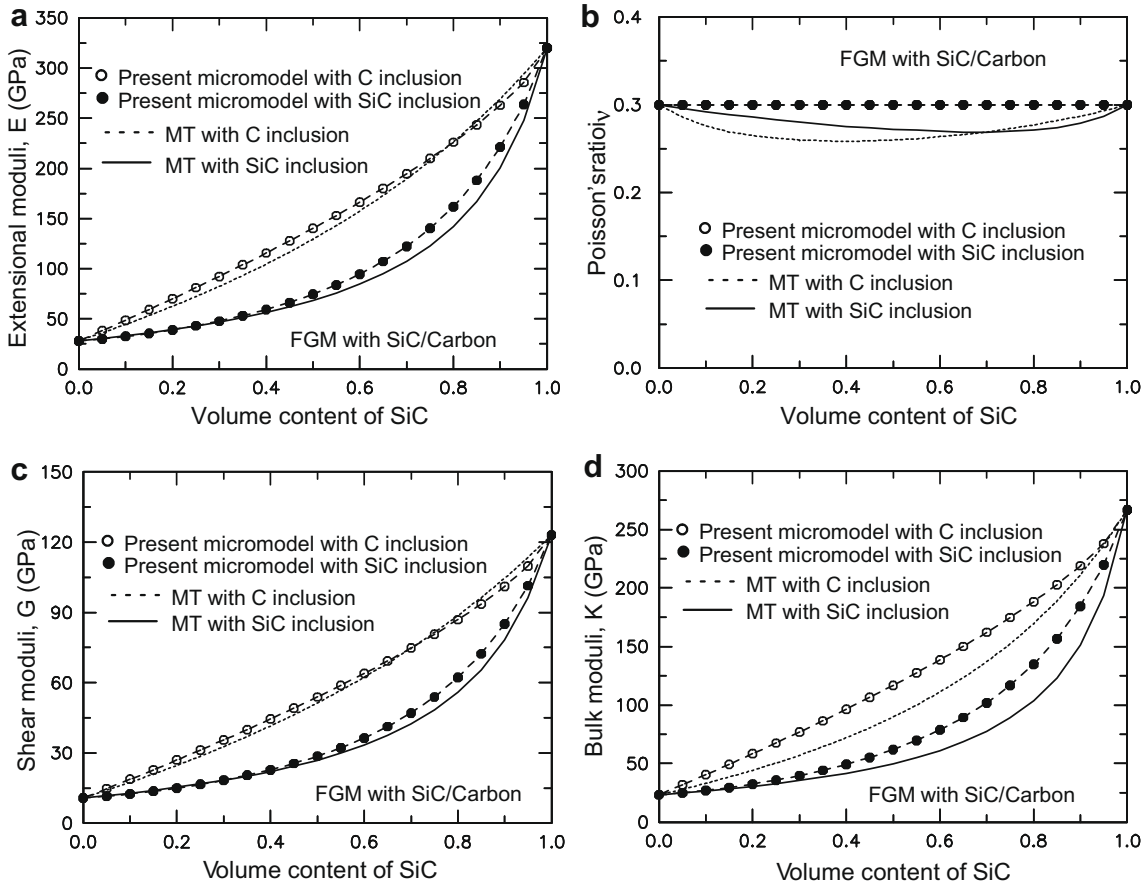


**Fig. 4.** Effective linear elastic moduli of FGM with linear through-thickness constituent gradation (MT – Mori and Tanaka model).

mal expansion (CTE) and thermal conductivity, are given in Fig. 5. Micromechanical models of Rosen and Hashin (1970) and Hatta and Taya (1985) are used for the effective CTE and thermal conductivity, respectively. The results also indicate that the different roles of the constituents as the inclusion and matrix can influence the overall thermal properties of the FGM.

The FGM model is divided into three zones through its thickness. The first zone considers SiC as inclusions (solid spherical particles) and C as homogeneous matrix, the second zone is the transition zone, and the third zone consists of C inclusions and SiC matrix. The effective thermo-viscoelastic properties in zones one and three are determined using the micromechanical model of solid spherical particle composites. The effective properties in the transition zone are obtained using Eq. (19). Fig. 6 illustrates effective elastic moduli (extensional moduli) of FGM having a linear through-thickness variation of the SiC and C constituents. Examples of FGM extensional elastic moduli with the limits of transition zone between 40% and 45% are shown. As discussed in Yin et al. (2007) and Moon et al. (2005), the location of the transition zone should be characterized from experiments, which could vary significantly for different FGM/composite systems. At the transition zone, contact among inclusions or interpenetrating between the constituents is observed. In heat conduction problems, the interpenetrating between the constituents, which is often referred to as percolation, accelerates the heat conduction process indicated by high effective thermal conductivity. Bao and Cai (1997) have discussed that for ceramic/metal composites, the percolation limit of the effective thermal conductivity is typically between 40% and 60%. Moon et al. (2005) have shown a discontinuity in the effective elastic modulus of Al–$Al_2O_3$ composites between 0% and 40%, 40–70%, and 70–100% volume content of Al. They also mentioned that the effects of interpenetrating between constituents and percolation on the overall responses of composites depend on the mismatch between the properties of the constituents. From a micromechanical modeling effort of a composite with same size of solid spherical inclusions, contact between inclusions can be avoided when the inclusion volume content is less than 56%. Unless the three FGM regions in Fig. 2 can be determined from experiments, the transition region is assumed within 40–60% of the composition of the constituents. It should be noted that interpenetrating between the constituents and percolation could also occur in composites with relatively low inclusion volume contents, e.g., 20%. This may be due to the material processing, which forms clusters of particles. A high ratio between the inclusion and matrix conductivities can also cause percolation at low particle content (Agari and Uno, 1985).

The effects of the constituent properties on the effective properties at the boundaries of the transition zone are examined. Fig. 7 illustrates the overall elastic moduli of FGM with several ratios of the constituent elastic properties, $E_1/E_2$: 2, 5, and 11.48. It is seen that, as the ratio increases, also the slope that measures a change in the effective elastic property with volume content in the transition zone increases. Similar effects should be expected for the thermal properties, as previously studied by Yin et al. (2007). The overall response of the FGM is also influenced by the variations of the constituent compositions along the graded directions which have been extensively studied, e.g., Praven and Reddy (1998). Fig. 8 illustrates the comparisons of the effective elastic moduli of SiC/C FGM with linear and cubic variations in the constituent compositions. The transition zone is chosen between 40% and 60% volume

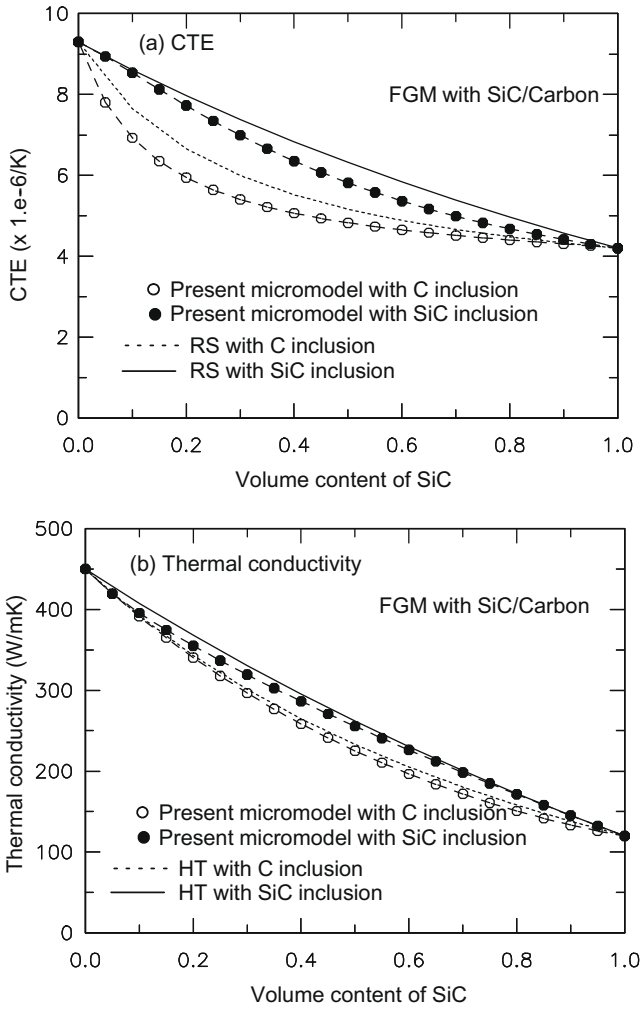


**Fig. 5.** Effective linear thermal properties (RS – Rosen and Hashin, HT – Hatta and Taya).

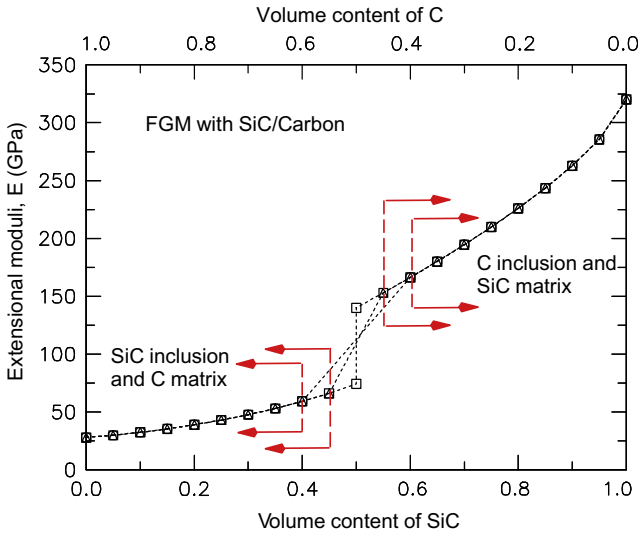


**Fig. 6.** Extensional elastic moduli of FGM with a transition zone.

contents of SiC. Significant differences in the location and slope of the transition zone in the FGMs with linear and cubic variations should be expected.

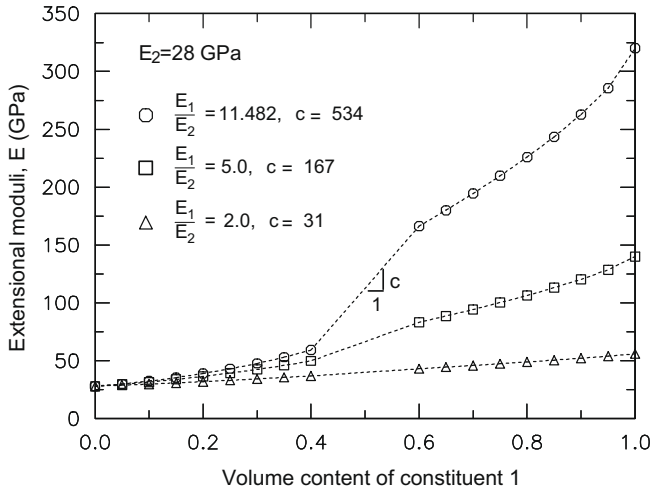


**Fig. 7.** Effects of constituent properties on the extensional moduli of FGM.

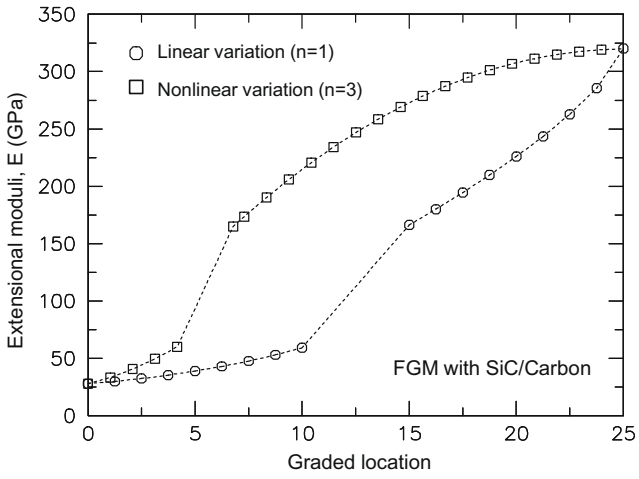


**Fig. 8.** Effect of variation in the constituent compositions on the extensional moduli of FGM.

### 4.2. Verification of the thermal and elastic properties

Effective thermal and elastic properties of FGMs are verified with existing experimental data. Experimental data reported by Parameswaran and Shukla (2000) on cenosphere/polyester FGMs are first used for comparisons. The elastic properties of the constituents are given in Table 2. Nonlinear variations in cenosphere's volume contents through the 25 cm thick FGMs are shown in Fig. 9. The maximum volume content of the cenosphere is 45% in which the transition zone can be neglected. The fitted functions for the cenosphere's volume contents in the two matrix systems are given by:

**Table 2**
Elastic properties of cenoshpere, polyester, polyester–plasticizer (Parameswaran and Shukla, 2000).

| Constituents | $E$ (GPa) | $\nu$ |
|---|---|---|
| Cenosphere | 6 | 0.35 |
| Polyester | 3.6 | 0.41 |
| Polyester–plasticizer | 2.5 | 0.33 |

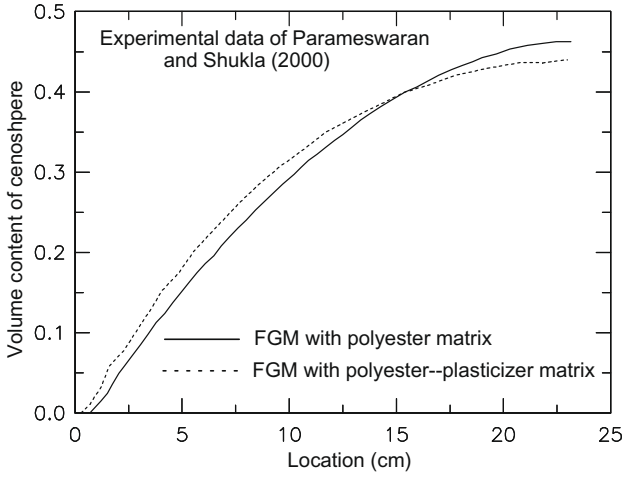


**Fig. 9.** Volume content of cenoshpere in polyester and polyester–plasticizer matrix.

$$\begin{aligned}&\text{polyester}: \ v_c = -8.35\times10^{-4}z^2 + 4.22\times10^{-2}z - 5.3\times10^{-2} \\ &\qquad z \geqslant 1\,\text{mm} \\ &\text{poly-plas}: \ v_c = -10^{-3}z^2 + 4.22\times10^{-2}z - 7.7\times10^{-2} \\ &\qquad z \geqslant 1\,\text{mm}\end{aligned} \tag{45}$$

The effective linear elastic properties of the FGM are determined using the present micromechanical model with cenosphere as the inclusions. Fig. 10 illustrates micromodel predictions of elastic moduli and Poisson's ratios of cenosphere/polyester and cenosphere/polyester–plasticizer FGM systems. Good predictions are observed. The elastic modulus obtained using the micromodel having particle interaction (Yin et al., 2004) is also shown for comparison. Next, experimental data of elastic properties of Ni3Al/TiC FGM reported by Zhai et al. (1993) are used for comparisons. The elastic properties of the constituents are given in Table 3. The studied FGM has a linear variation in the composition of the constituents. Fig. 11 shows predictions of the elastic moduli and Poissons' ratio. The transition zone is considered between 40% of Ni3Al volume content and 40% of TiC volume content. Due to a low ratio in the elastic properties of the constituents, the discontinuities in the effective properties between the two bounds of the transition zone is relatively small. Unlike in the previous study (Fig. 6), pronounced discontinuities are due to significant mismatches in the properties of the constituents. Predictions from the present micromechanical model match very well with the ones obtained from the micromodel with particle interactions (Yin et al., 2004). In this study, instead of considering particle interactions, which is essential for composites with high inclusion volume contents, a simplified micromodel with periodic boundary conditions and an interchange of the inclusion and matrix constituents are employed.

Effective CTEs of FGMs obtained using the present micromodel are also compared with experimental data. Two FGMs are studied, i.e., Mo/$SiO_2$ (Ishibashi et al., 2000) and Al/$Al_2O_3$ (Neubrand et al., 2002). The linear elastic moduli and CTEs of the constituents at a fixed temperature are reported in Table 4. Following Yin et al. (2007), the volume content of the Mo inclusions is:

$$\begin{aligned}&v_{\text{pf}}^{\text{Mo}} = 0.2\left(\exp\left(-28(r-0.085)^2\right) - 0.1r + 0.1\right) \\ &r = z/h \quad 0 \leqslant z \leqslant h \quad h = 2.5\,\text{cm}\end{aligned} \tag{46}$$

The maximum volume content of Mo is less than 0.3. The FGM having Al/$Al_2O_3$ constituents also shows maximum volume content of 30%. Thus, in both FGM systems, transition zones are neglected. Fig. 12 illustrates comparisons of effective CTEs of the two FGMs

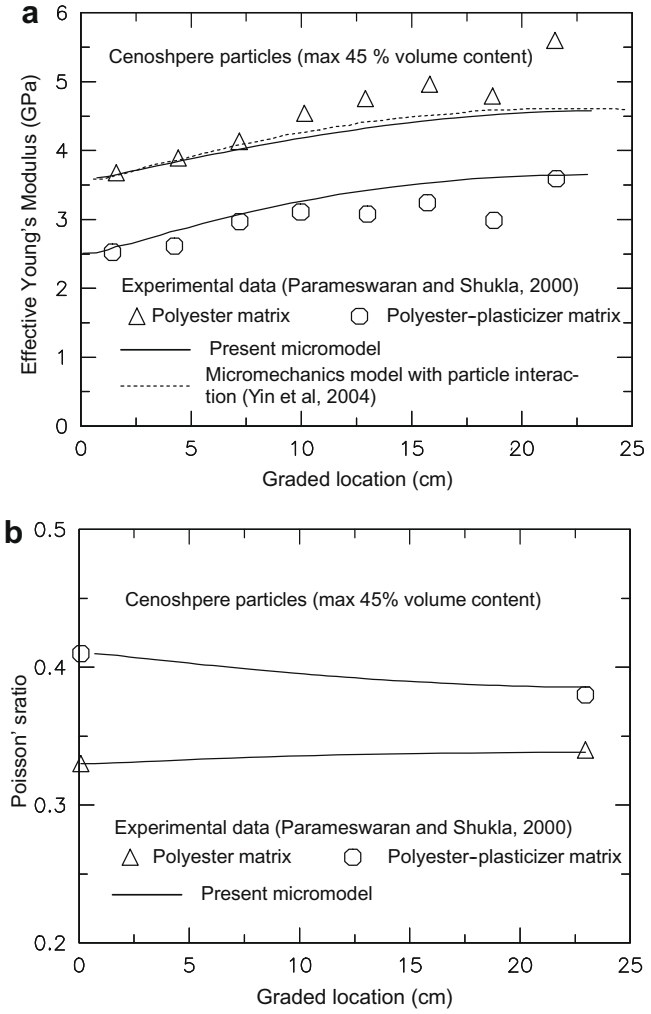


**Fig. 10.** Prediction of (a) elastic moduli and (b) Poisson's ratio of cenoshpere based FGM.

**Table 3**
Elastic properties of Ni3Al and TiC (Zhai et al., 1993).

| Constituents | $E$ (GPa) | $v$ |
|---|---|---|
| Ni3Al | 199 | 0.295 |
| TiC | 460 | 0.19 |

at a constant temperature. Responses from the micromodel match well with experimental data and also with the micromodel of particle interaction. In order to examine the effect of temperature on the CTE of the Al/$Al_2O_3$ FGM, temperature-dependent properties of the aluminum constituent, which are taken from Aboudi (1985), are considered. Fig. 13 shows the variations of elastic modulus and CTE of aluminum with temperature. Linear and quadratic polynomial functions are used to fit the CTE and elastic modulus, respectively. Effective CTE of the Al/$Al_2O_3$ FGM is given in Fig. 14. The limits of the transition zone are between 40% and 60%. The effect of temperature on the effective CTE is more pronounced in the region with relatively high contents of aluminum which is expected. The mismatch in the constituent properties increases with increasing temperatures which results in a higher slope of the transition zone.

Next, CTEs of FGM having $Al_2O_3$ and NiCr constituents at temperatures: 0–1200 °C are studied. The linear elastic moduli and CTE of the constituents at temperature 10 °C are reported in Table

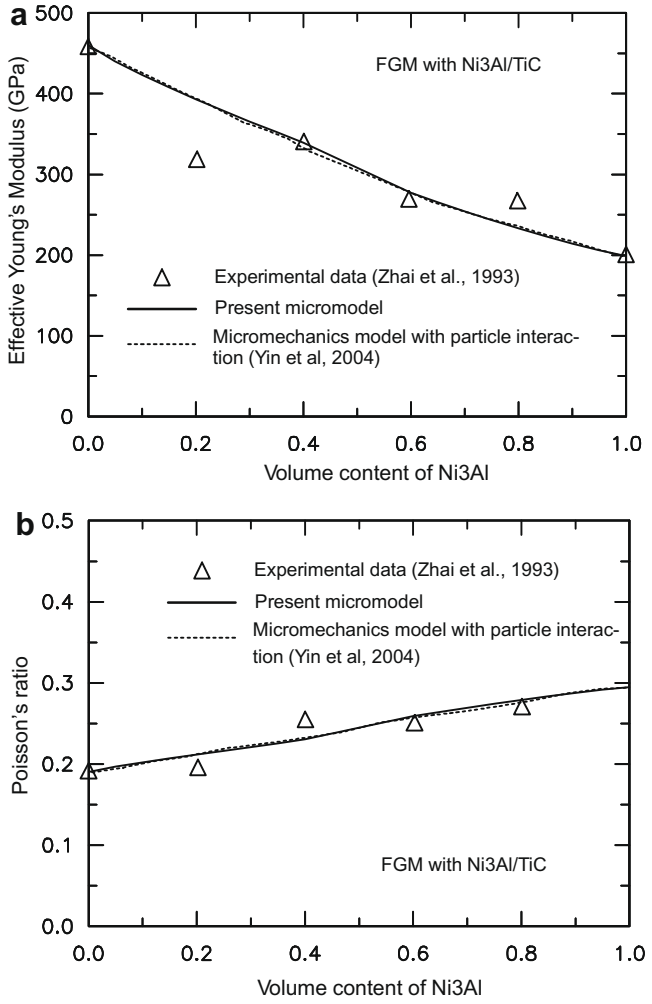


**Fig. 11.** Prediction of (a) elastic moduli and (b) Poisson's ratio of FGM with Ni3Al/TiC.

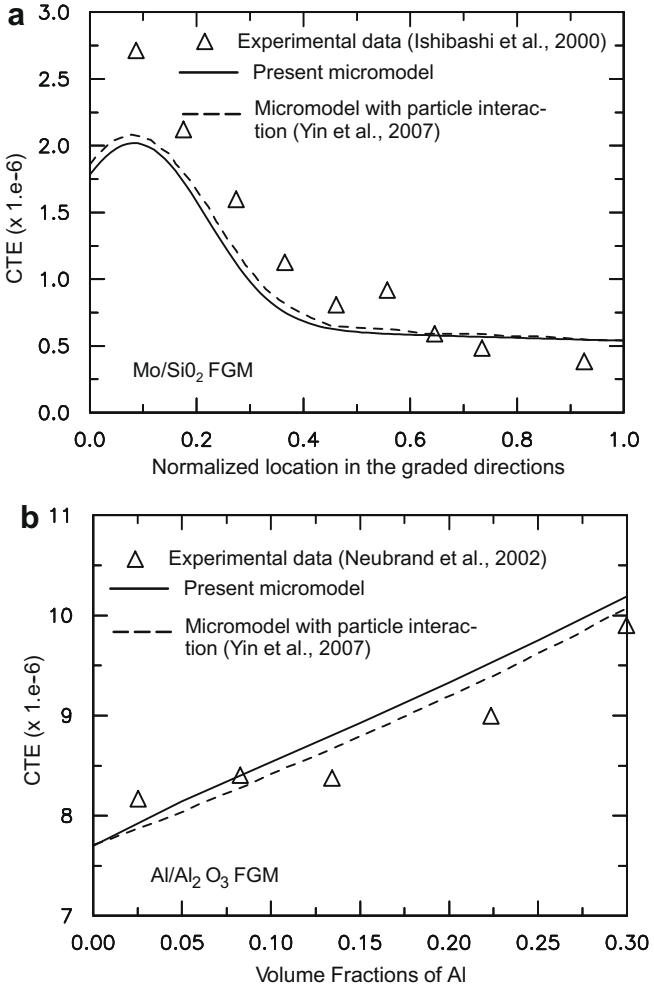


**Fig. 12.** Linear CTE predictions of FGM systems: (a) $Mo/SiO_2$ and (b) $Al/Al_2O_3$.

**Table 4**
Linear thermo-elastic properties of $Mo/SiO_2$ and $Al/Al_2O_3$.

| Constituents | $E$ (GPa) | $\nu$ | $\alpha$ ($10^{-6}$/K) |
|---|---|---|---|
| Mo | 324 | 0.31 | 5.1 |
| $SiO_2$ | 80.4 | 0.18 | 0.54 |
| Al | 69 | 0.33 | 23.1 |
| $Al_2O_3$ | 390 | 0.2 | 7.7 |

5. The CTE of the NiCr constituent varies with temperatures, which is experimentally studied by Petrus and Ferguson (1997), while the CTE of the $Al_2O_3$ constituent is independent of temperature. The temperature-dependent CTE of the NiCr is expressed as:

$$\alpha_{NiCr} = (12 + 0.002T) \times 10^{-6}/C \quad (47)$$

Fig. 15 presents predictions of the effective CTEs at various temperatures for the FGMs having $Al_2O_3$ volume contents of 0%, 20%,40%, and 60%. At 60% $Al_2O_3$ volume content, the effective CTE is obtained using the micromodel with 40% NiCr particles dispersed in homogenous $Al_2O_3$ matrix. The present micromechanical model is capable of predicting temperature-dependent CTEs. A micromechanical model prediction without interchange in the inclusion and matrix constituents (using 60% $Al_2O_3$ particles in the micromodel) is also reported (dashed line). Although the dashed-line slightly over predicts the experimental data, the mismatch is negligible. The insignificant mismatch is due to a relatively low ratio of the constituent properties and moderate volume content of $Al_2O_3$. It has previously been shown (Fig. 5a) that the high ratio of the constituents can result in a significant mismatch in the effective CTEs with altering the inclusion and matrix constituents, although the composition of the constituents are kept constant.

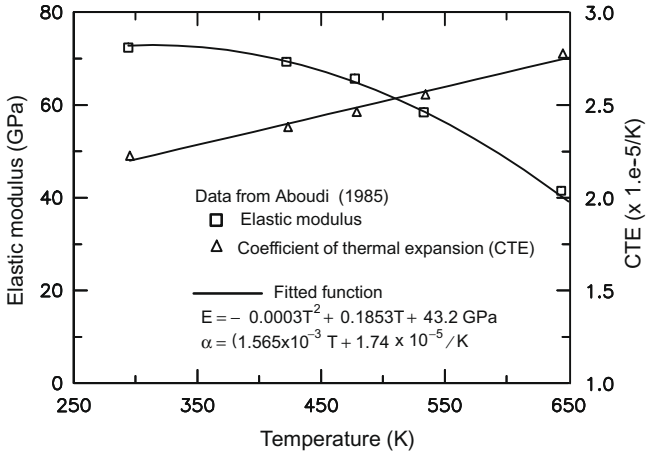


**Fig. 13.** Temperature-dependent properties of aluminum.

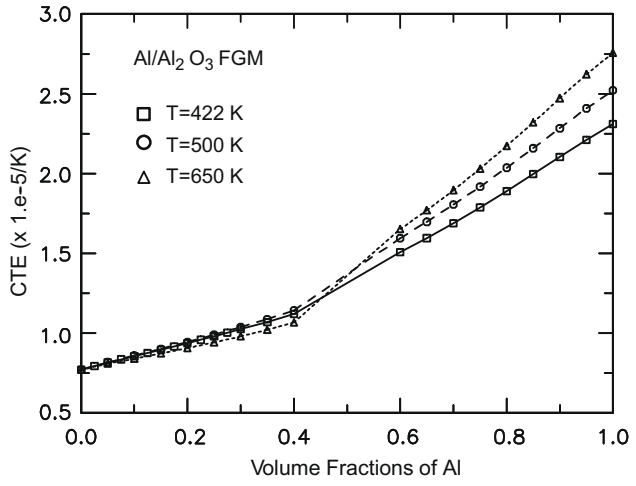


**Fig. 14.** CTE of $Al/Al_2O_3$ FGM at various temperatures.

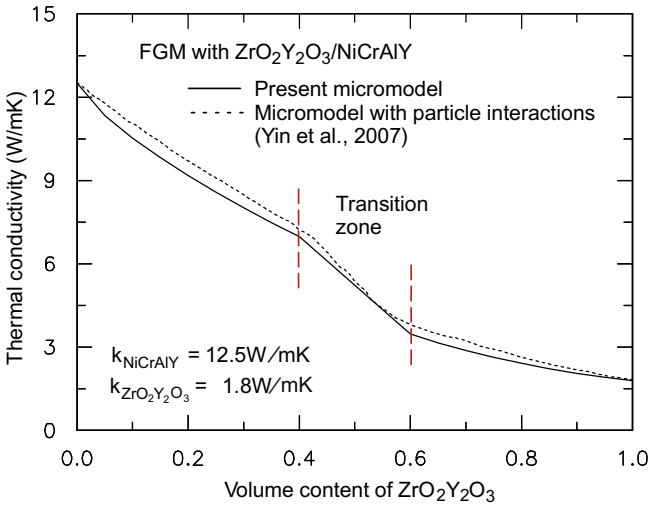


**Fig. 16.** Thermal conductivity predictions of $ZrO_2Y_2O_3$/NiCrAlY FGM.

**Table 5**
Linear thermo-elastic properties of $Al_2O_3$ and NiCr at 10 °C.

| Constituents | $E$ (GPa) | $\nu$ | $\alpha$ ($10^{-6}$/K) |
|---|---|---|---|
| $Al_2O_3$ | 380 | 0.26 | 8.6 |
| NiCr | 156 | 0.27 | 12.0 |

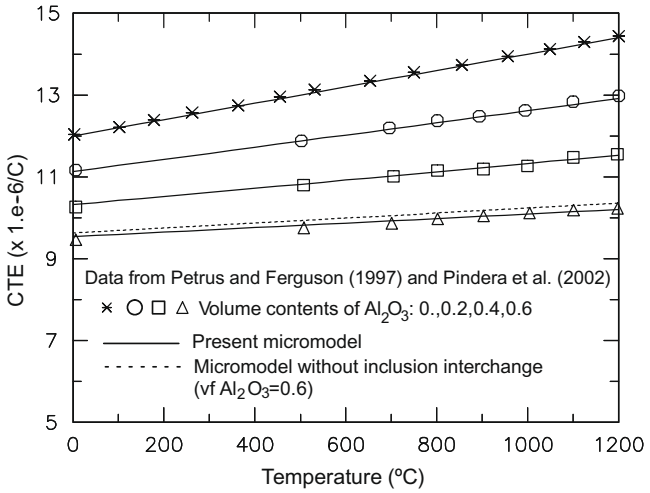


**Fig. 15.** CTE prediction of $Al_2O_3$/NiCr FGM.

The effective thermal conductivities of FGMs obtained from the present micromodel are also compared to the ones of Yin et al. (2007), in which particle interactions are incorporated. Fig. 16 illustrates a good match between the two models on predicting effective thermal conductivities of FGM having NiCrAlY/$ZrO_2Y_2O_3$ constituents. The transition zone is assumed between 40% and 60% volume fractions of the $ZrO_2Y_2O_3$ constituent.

### 4.3. Effects of temperature and time on the overall responses of FGM

The effects of time and temperature on the overall thermal and elastic properties of FGMs are studied. The present micromechanical model is used to provide effective properties of FGMs. The presented studies consider a linear variation in compositions of the constituents in FGMs. The first study deals with relaxation moduli of cenosphere/polyester FGM. The linear elastic properties of the constituents are given in Table 2. The elastic modulus of the polyester constituent relaxes with time while the properties of the cenosphere are constant. Time-dependent creep compliance of the polyester is taken from Muliana (2004) and it is given in Table 6. These values are fitted using exponential function in Eq. (7) from 3600-s creep tests. Fig. 17 illustrates relaxation moduli of previously studied cenosphere/polyester FGM. The moduli along the graded location relax with different rates due to different compositions of the constituents. Relaxation occurs faster at early times with decreasing rates at later times. After about 2 h, the moduli at the distance 1 cm (polyester rich area) decreases by 16% from

**Table 6**
Calibrated Prony series coefficients for polyester (Muliana, 2004).

| $n$ | $\lambda_n$ ($s^{-1}$) | $D_n \times 10^{-6}$ ($ksi^{-1}$) | $D_n$ ($GPa^{-1}$) |
|---|---|---|---|
| 1 | 1 | 143.76 | 0.0208 |
| 2 | $10^{-1}$ | 130.99 | 0.019 |
| 3 | $10^{-2}$ | 137.05 | 0.0199 |
| 4 | $10^{-3}$ | 140.83 | 0.0204 |
| 5 | $10^{-4}$ | 345.00 | 0.05 |
| 6 | $10^{-5}$ | 580.00 | 0.0841 |

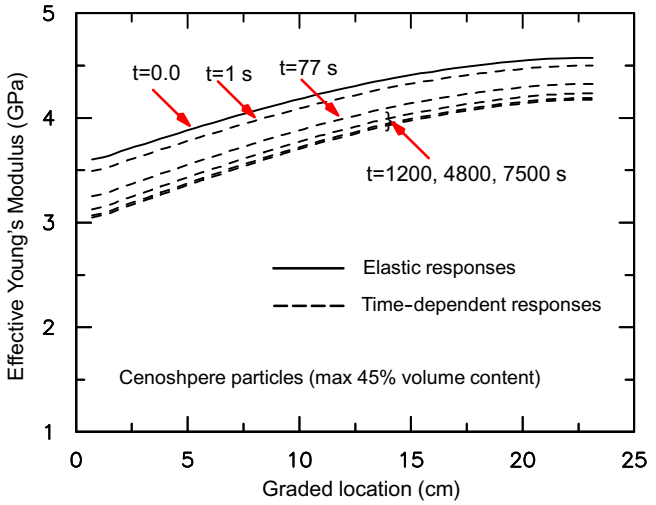


**Fig. 17.** Relaxation moduli of cenosphere/polyester FGM.

its initial elastic value, while at the distance 23 cm the moduli has decreased by 8% from its initial elastic value. The FGM model does not include a transition zone since the maximum volume content of the cenosphere particles is 45% (Parameswaran and Shukla, 2000). The second study analyzes relaxation moduli of FGMs having $Al_2O_3$ and NiCr constituents. The elastic modulus of NiCr constituent is assumed to relax with time while the one of $Al_2O_3$ constituent is constant. Fig. 18 shows relaxation moduli of the FGM obtained using the present micromodel. The transition zone is modeled between 40% and 60% volume fractions of $Al_2O_3$ constituent. As expected, the effective moduli along the graded locations in the FGM relax with time at different rates. The difference in moduli of the two constituents increases during relaxation process, which results in higher jumps in the effective moduli between the two bounds of the transition zone.

A sequentially coupled analysis of heat conduction and deformation in an FGM made of zirconia and Ti6Al constituents is performed. Thermal and elastic properties of the constituents at a particular location depend on the temperature at that location (nonlinear analyses). The temperature dependent properties of the constituents are taken from Reddy and Chin (1998). Fig. 19 illustrates temperature profiles during transient heat transfer analyses in the FGM panel. The transition zone is taken within 45–55% volume content of zirconia. The temperature dependent thermal conductivities of the constituents accelerate the heat conduction process. Steady state (SS) time for the nonlinear analyses is 325 s while for the linear analyses is 1390 s. Thus, assuming constant thermal conductivities can lead to significant errors in determining temperature profiles. These errors will be accumulated in the stress analyses of FGM. Next, the FGM panel is subjected to a constant uniaxial pressure along its thickness direction. Heat conduction (Fig. 19a) is then performed on the stressed FGM. Fig. 20a and b presents axial displacements and in-plane shear stresses in the FGM panels at various times. It is seen that the displacements and shear stresses vary with increasing time due to the non-constant (temperature dependent) elastic properties of the constituents.

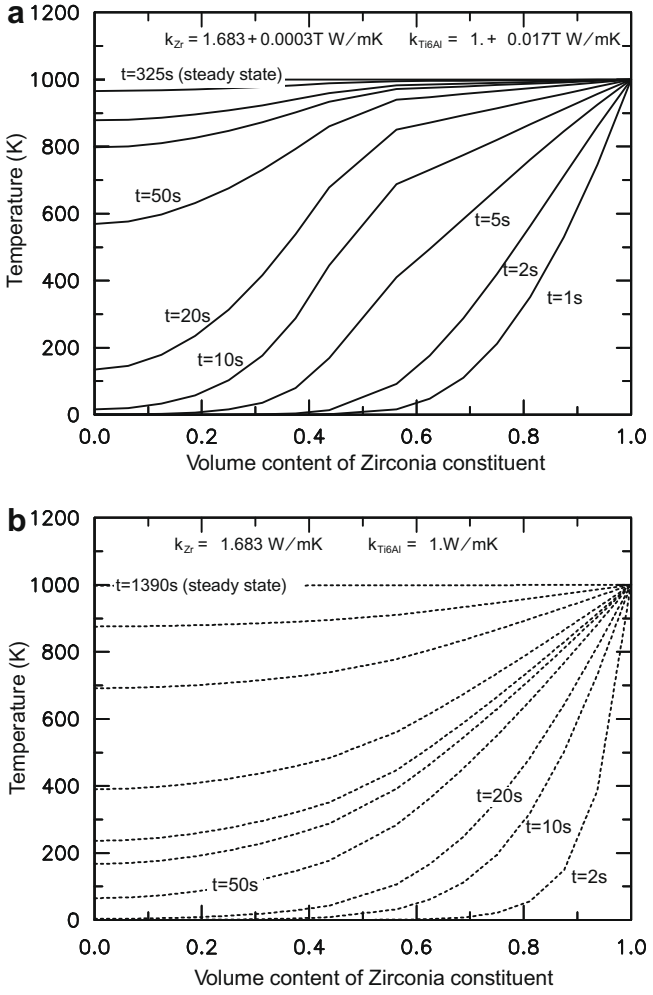


**Fig. 19.** Temperature profiles for FGM of Zr/Ti6Al constituents: (a) nonlinear and (b) linear.

## 5. Conclusions

This study presents a micromechanical modeling framework for predicting thermal properties and thermo-viscoelastic behaviors of FGMs graded in one direction. The studied FGM comprises of two constituents: one constituent acts as discontinuous inclusions and the other constituent acts as homogeneous matrix. The microstructures of the FGM are idealized as solid spherical particles spatially distributed in homogeneous matrix. The mechanical properties of each constituent are allowed to vary with temperature and time while the thermal properties are allowed to vary with temperature. The FGM model includes a transition zone where the inclusion and matrix constituents are not well defined. At the transition zone, an interchange between the inclusion and matrix constituents takes place such that the maximum inclusion volume contents are less than 50%. This study also assumes a symmetrical constituent-inversion before and after the transition zone. This is done to simplify the micromechanical formulation such that the effect of microstructural details, e.g., particle interactions or interpenetrating between the constituents, can be minimized. Particle interactions can significantly affect overall performance of composites when high inclusion volume contents are considered. Furthermore, for composite systems having high volume contents of particles (inclusion), i.e., above 60%, it is not possible to have all particles/inclusions fully surrounded by continuous matrix. In this situation, more discontinuities exist in the matrix. It should be noted that degree of mismatches in the properties of constituents also determines the overall behaviors of FGM. Furthermore, when the constituents exhibit time and temperature-dependent behaviors, the mismatches in the constituent properties change during deformations. Available experimental data and analytical solutions in the literature are used to verify the micromechanical

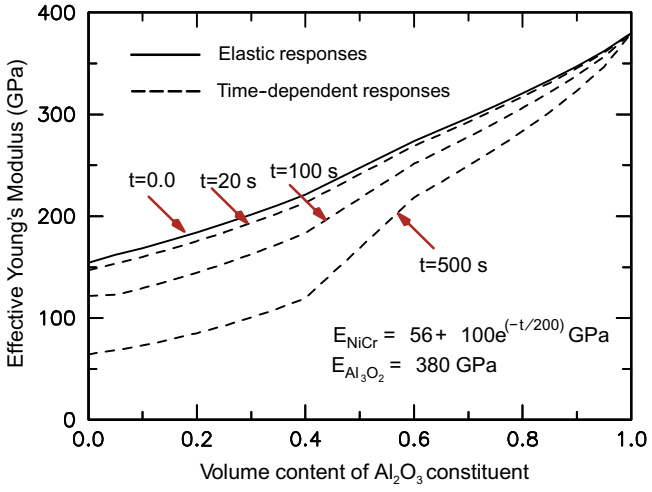


**Fig. 18.** Relaxation moduli of $Al_2O_3$/NiCr FGM.

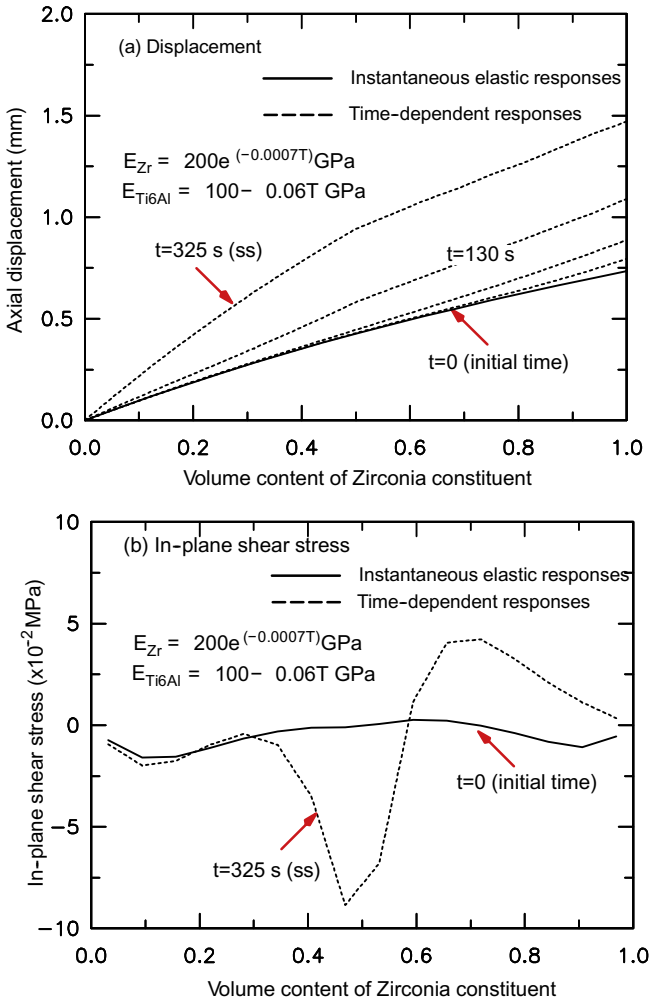


**Fig. 20.** Responses of Zr/Ti6Al FGM subject to conduction of heat and constant axial stress through the thickness direction: (a) axial displacement and (b) in-plane shear stress.

formulation. The present micromodel is suitable for analyzing thermo-mechanical responses of FGM having field and time dependent constituent properties.

## Acknowledgment

This research is sponsored by the National Science Foundation under Grant No. 0546528.

## References

Aboudi, J., 1985. Inelastic behavior of metal–matrix composites at elevated temperature. Int. J. Plasticity 1, 359–372.
Aboudi, J., Pindera, M.J., Arnold, S.M., 1996. Thermoelastic theory for the response of materials graded in two directions. Int. J. Solids Struct. 33, 931–966.
Aboudi, J., Pindera, M.J., Arnold, S.M., 1999. Higher order theory for functionally graded materials. Composite B 30, 777–832.
Alberola, N.D., Mele, P., 1996. Viscoelasticity of polymers filled by rigid or soft particles: theory and experiment. Polym. Compos. 17, 751–759.
Agari, Y., Uno, T., 1985. Thermal conductivity of polymers filled with carbon materials. J. Appl. Polym. Sci. 30, 2225–2235.
Bao, G., Cai, H., 1997. Delamination cracknig in functionally graded coating/metal substrate systems. Acta. Materialia. 45, 1055–1066.
Boley, B.A., Weiner, J.H., 1997. Theory of Thermal Stresses. Dover, New York.
Gasik, M.M., 1998. Micromechanical modeling of functionally graded materials. Comput. Mater. Sci. 13, 42–55.
Hatta, H., Taya, M., 1985. Effective thermal conductivity of misoriented short fiber composites. J. Appl. Phys. 58, 2478–2486.
Haj-Ali, R.M., Muliana, A.H., 2004. Numerical finite element formulation of the Schapery nonlinear viscoelastic material model. Int. J. Numer. Method Eng., 59.
Ishibashi, H., Tobimatsu, H., Matsumoto, T., Hayashi, K., Tomsia, A.P., Saiz, E., 2000. Characterization of Mo–$SiO_2$ functionally graded materials. Metall. Mater. Trans. A. 31A, 2000–2299.
Mukherjee, S., Paulino, G., 2003. The elastic–viscoelasitc correspondence principle for functionally graded materials: revisited. ASME J. Appl. Mech. 70, 359–363.
Muliana, A.H., 2004. Ph.D. Thesis, Georgia Institute of Technology.
Muliana, A.H., 2007. Multi-scale framework for the thermo-viscoelastic analyses of polymer composites. Mech. Res. Commun. 34, 561–567.
Muliana, A.H., Khan, K.A., 2008. A time integration algorithm for thermo-rheologically complex polymers. Comput. Mater. Sci. 41, 576–588.
Muliana, A.H., Kim, J.S., 2007. A concurrent micromechanical model for nonlinear viscoelastic behaviors of composites reinforced with solid spherical particles. Int. J. Solids Struct. 44, 6891–6913.
Muliana, A.H., Sawant, S.,, in press. Viscoelastic responses of polymer composites with temperature and time dependent constituents. Acta Mech.
Moon, R.J., Tilbrook, M., Hoffman, M., Neubrand, A., 2005. Al–$Al_2O_3$ Composites with interpenetrating network structures: composite modulus estimation. J. Am. Ceram. Soc. 88, 666–674.
Neubrand, A., Chung, T.J., Rodel, J., Steffler, E.D., Fett, T., 2002. Residual stresses in functionally graded plates. J. Mater. Res. 17, 2912–2920.
Noda, N., 1999. Thermal stresses in functionally graded materials. J. Therm. Stress 22, 477–512.
Ostoja-Starzewski, M., Jasiuk, I., Wang, W., Alzebdeh, K., 1996. Composite with functionally graded interphases: mesocontinuum concept and effective transverse conductivity. Acta Metall. 44, 2057–2066.
Parameswaran, V., Shukla, A., 2000. Processing and characterizing of a model functionally gradient material. J. Mater. Sci. 35, 21–29.
Pindera, M.J., Aboudi, J., Arnold, S., 2002. Analysis of spallation mechanism in thermal barrier coatings with graded bond coats using the higher-order theory of FGM. Eng. Fract. Mech. 69, 1587–1606.
Petrus, G.J., Ferguson, B.L., 1997. A software tool to design thermal barrier coatings: a technical note. J. Therm. Spray Technol. 6 (1), 29–34.
Praven, G.N., Reddy, J.N., 1998. Nonlinear transient thermoelastic analyses of functionally graded ceramic–metal plates. Int. J. Solids Struct. 35, 4457–4476.
Praven, G.N., Reddy, J.N., 1999. Thermoelastic analyses of functionally graded ceramic–metal cylinder. ASCE J. Eng. Mech. 125, 1259–1267.
Reddy, J.N., Cheng, Z.Q., 2001. Three-dimensional thermomechanical deformations of functionally graded rectangular plates. Eur. J. Mech. A 20, 841–855.
Reddy, J.N., Chin, C.D., 1998. Thermomechanical analysis of functionally graded cylinders and plates. J. Therm. Stress 21, 593–626.
Reiter, T., Dvorak, G.J., Tvergaard, V., 1997. Micromechanical models for graded composite materials. J. Mech. Phys. Solids 45, 1281–1302.
Rosen, B.W., Hashin, Z., 1970. Effective thermal expansion coefficient and specific heats of composite materials. Int. J. Eng. Sci. 8, 157–173.
Sawant, S., Muliana, A., 2008. A thermo-mechanical viscoelastic analysis of orthotropic media. Compos. Struct. 83, 61–72.
Shabana, N., Noda, N., 2008. Numerical evaluation of the thermomechanical effective properties of a functionally graded materials using the homogenization method. Int. J. Solids Struct. 45, 3494–3506.
Shen, H.S., Noda, N., 2005. Postbuckling of FGM cylindrical shell under combined axial and radial mechanical loads in thermal environments. Int. J. Solids Struct. 42, 4641–4662.
Torquato, S., 2002. Random Heterogeneous Materials: Microstructure and Macroscopic Properties. Springer, New York.
Ueda, S., 2002. Thermal shock analysis of functionally graded materials by micromechanical model. JSME Int. J. 45, 138–145.
Ueda, S., Gasik, M., 2000. Thermal–elasto-plastic analysis of W–Cu functionally graded materials subjected to a uniform heat flow by micromechanical model. J. Therm. Stress 23, 395–409.
Vel, S.S., Batra, R.C., 2003. Three-dimensional analysis of transient thermal stresses in functionally graded plates. Int. J. Solids Struct. 40, 7181–7196.
Wineman, A., Rajagopal, K.R., 2001. Mechanical Responses of Polymers: An Introduction. Cambridge University Press, Cambridge.
Yang, Y.Y., 2000. Time-dependent stress analyses in functionally graded materials. Int. J. Solids Struct. 37, 7593–7608.
Yin, H.M., Sun, L.Z., Paulino, G.H., 2004. Micromechanics-based elastic model for functionally graded particulate materials with particle interactions. Acta Mater. 52, 3535–3543.
Yin, H.M., Paulino, G.H., Buttlar, W.G., Sun, L.Z., 2007. Micromechanics-based thermoelastic model for functionally graded particulate materials with particle interactions. J. Mech. Phys. Solids 55, 132–160.
Zhai, P.C., Jiang, C.R., Zhang, Q.J., 1993. Ceramic Transactions: Functionally Gradient Materials. The American Ceramic Society. p. 449.
Zhai, P.C., Chen, G., Zhang, Q.J., 2005. Creep property of functionally graded materials. Mater. Sci. Forum, 599–604.
Zhou, Y.C., Hashida, T., 2001. Coupled effects of temperature gradient and oxidation on thermal stress in thermal barrier coating system. Int. J. Solids Struct. 38, 4235–4264.
Zhou, Y.C., Hashida, T., 2002. Thermal fatigue failure induced by delamination in thermal barrier coating. Int. J. Fatigue 24, 407.